processes

MDPI

Article

To Promote the Catalytic Ozonation of Typical VOCs by Modifying NiO with Cetyltrimethylammonium Bromide

Chenguang An, Xinxin Jiang, Wei Hong, Ye Sun * and Tianle Zhu

Department of Environmental Science and Engineering, School of Space and Environment, Beihang University, Beijing 100191, China; ancg2020@buaa.edu.cn (C.A.); jxx@buaa.edu.cn (X.J.); weihongwh@buaa.edu.cn (W.H.); zhutl@buaa.edu.cn (T.Z.)

* Correspondence: suny@buaa.edu.cn

Abstract: A series of mesoporous NiO catalysts with high specific surface area were prepared by a simple hydrothermal method and modified by cetyltrimethylammonium bromide (CTAB) as the crystal structure directing regent. The characterization with SEM, XRD, BET, and H_2-TPR results demonstrated that the introduction of CTAB effectively improved the dispersion, specific surface area, and pore volume and redox ability of NiO, and thus exposed more active sites. Meanwhile, the NiO catalyst with a CTAB/$NiSO_4 \cdot 6H_2O$ molar ratio of 2/3 exhibited the better catalytic ozonation performance of toluene, formaldehyde, methanol, and ethyl acetate than NiO. The in-situ DRIFTS elucidated the reaction path of catalytic ozonation of toluene and indicated that the introduction of CTAB facilitated the complete oxidation of by-products into CO_2 and H_2O.

Keywords: catalytic ozonation; typical VOCs; NiO catalyst; CTAB modification

Citation: An, C.; Jiang, X.; Hong, W.; Sun, Y.; Zhu, T. To Promote the Catalytic Ozonation of Typical VOCs by Modifying NiO with Cetyltrimethylammonium Bromide. *Processes* **2023**, *11*, 1893. https://doi.org/10.3390/pr11071893

Academic Editor: Albert Renken

Received: 25 May 2023
Revised: 14 June 2023
Accepted: 20 June 2023
Published: 23 June 2023

1. Introduction

Volatile organic compounds (VOCs) are a class of organic compounds with boiling points between 50–260 °C at standard atmospheric pressure, and widely originated from fossil fuel combustion, chemical industry, and various waste emissions [1–6]. These VOCs can participate in photochemical reactions, causing environmental problems and serious health problems, and even cancer [7,8]. To control air pollution more effectively, China has issued a series of more stringent environmental policies to reduce VOCs emissions [9]. Consequently, there is an urgent need to develop the technologies that can effectively control VOCs emissions [10,11].

Compared to traditional VOCs control technologies, catalytic ozonation is considered to be one of the most promising technologies for VOCs removal with the decrease in O_3 production cost because of its mild reaction condition [8,10,12]. In addition, it has a wide adaptability to the types and concentrations of VOCs [13]. However, there exist wide differences in the properties and concentrations of VOCs in actual industrial exhaust gases, which is posing a challenge to the applicability and universality of catalytic ozonation catalysts [14,15].

The catalytic ozonation of VOCs over the transition metal oxides, such as Co, Ce, Ni, Cu, Zn, Mg, and Mn, has widely been investigated at low or room temperature [8,16,17]. The catalytic activity varies greatly for different transition metal oxides. Among them, nickel oxide (NiO_x) is thought to be a valuable catalyst of catalytic ozonation of VOCs because of its valence diversity, controllable crystal morphology, easy formation of oxygen vacancies, and high specific surface area. Additionally, ozone can easily adsorb on the surface of NiO_x and thus generate hydroxyl radicals (OH) and superoxide ions (O_2^-) through radical chains [18]. Moreover, it has been reported that NiO_x with over stoichiometric oxygen can efficiently degrade various compounds [19,20], and exhibit good catalytic activity for many difficult-to-degrade VOCs at low temperature [13,20,21].

On the other hand, suitable surfactants can passivate the nanoparticle surface and reduce the agglomeration, which is helpful to improve the catalytic activity of the catalysts [22]. Cetyltrimethylammonium bromide (CTAB), acting as a capping agent and a structure-directing agent, can effectively promote anisotropic growth of crystals to obtain nanocrystals of different sizes and shapes [23]. Using the CTAB co-precipitation method, Navneet Kaur et al. [23] controlled the specific surface area of NiO nanoparticles, which resulted in significant improvement in their specific surface area and catalytic activity of reactive blue 81 and Coomassie brilliant blue R-250 dyes. In a related study, Tong et al. [24] synthesized $LiNi_{0.8}Co_{0.1}Mn_{0.1}O_2$ material with CTAB assistance, which exhibited enhanced crystallinity and cycle stability due to reduced agglomeration.

In this work, a series of mesoporous NiO catalysts were obtained by adding different amounts of CTAB as the directing agent and were used for the catalytic ozonation of VOCs. Various characterizations and performance evaluations suggested that the introduction of CTAB could modify the morphology and particle size of NiO, and thus increase its specific surface area, and enhance catalytic activity. Moreover, we further explored the reaction pathway of the catalytic ozonation of toluene and investigated the catalytic degradation effect of the modified NiO catalysts on other typical VOCs, including formaldehyde (aldehydes), methanol (alcohols), and ethyl acetate (esters).

2. Material and Methods

2.1. Materials

Nickel sulfate hexahydrate, urea, cetyltrimethylammonium bromide (CTAB), toluene, formaldehyde, methanol, and ethyl acetate were purchased from Shanghai Aladdin Biochemical Technology Co., Ltd. (Shanghai, China). Among them, toluene, methanol, formaldehyde, and ethyl acetate were all chromatographically pure.

2.2. Preparation of Catalyst

A series of NiO catalysts were prepared using the hydrothermal method and modified by changing the amount of cetyltrimethylammonium bromide (CTAB) as the crystal structure directing regent. An amount of 13.15 g $NiSO_4{\cdot}6H_2O$ and 0 g, 6 g, 12 g, and 18 g CTAB (with CTAB/$NiSO_4{\cdot}6H_2O$ molar ratios of 0, 1/3, 2/3, and 1), respectively, as well as 6.006 g CH_4N_2O, being used to maintain the alkaline condition, were dissolved in 300 mL of deionized water and magnetically stirred at 700 rpm for 30 min until a uniform green solution was obtained. The mixture solution was transferred to a 500 mL polytetrafluoroethylene reactor, sealed, and placed in a vacuum oven for hydrothermal reaction at 180 °C for 12 h. After the reactor was naturally cooled to room temperature, the suspension was filtered using a vacuum pump and washed with deionized water until the filtrate pH was neutral. The obtained solid was then dried at 110 °C overnight and calcined in air at 400 °C for 6 h to obtain CTAB/NiO-Z (Z = 0, 1/3, 2/3, and 1, corresponding to CTAB/$NiSO_4{\cdot}6H_2O$ molar ratios of 0, 1/3, 2/3, and 1) catalysts, respectively. Finally, the above catalyst powders were pressed into tablets under 20 ± 5 MPa, then ground, and sieved to obtain 40–60 mesh particles for catalytic performance evaluation.

2.3. Characterization

The morphology of the catalysts was observed utilizing a ZEISS scanning electron microscope (SEM). An X-ray powder diffractometer (XRD, Bruker D8 type, Bruker Corporation, Billerica, MA, USA) was used to analyze the crystal structure of the catalyst in a scanning range of 10°–90° with a scanning speed of 2°/min and a step size of 0.02°. The obtained catalyst lattice parameters were refined using the Jade-6 software. The specific surface area and pore size distribution of the catalysts were determined at Brunel Emmett Taylor (BET, ASAP2020, Micromeritics Instrument Corp., Norcross, GA, USA) by a gas absorption technique. N_2 adsorption and desorption experiments were carried out at 77 K for specific surface area measurements. In order to remove surface adsorbed impurities, the catalyst underwent a pre-treatment process under vacuum conditions at

250 °C for a duration of 3 h. Additionally, pore size distribution and pore volume of the catalyst were calculated by the BJH analysis method. To investigate the reduction performance of the catalyst, H_2 programmed temperature rise reduction (H_2-TPR) experiments were conducted on an AutoChem 2920 analyzer (Micromeritics Instrument Corporation, USA). The reaction mechanism of catalytic ozonation of toluene was determined by analyzing the oxidation products using an In Situ DRIFTS technique on a Thermo Fisher Scientific (Waltham, MA, USA) Nicolet 6700 FTIR instrument. The scanning range was 400–4000 cm^{-1} with an instrumental resolution of 4 cm^{-1}.

2.4. Performance Evaluation of Catalytic Ozonation

All catalytic ozonation experiments were performed in a fixed quartz tube reactor with an inner diameter of 5.8 mm at standard atmospheric pressure and 30 °C. The simulated reaction gas is composed of O_3, VOCs (toluene, formaldehyde, methanol, and ethyl acetate), and water vapor, with compressed air as the balance gas. The total flow rate of the simulated reaction gas was controlled at 1 L/min by the mass flow controller, where O_3 was generated by synthesis gas (5% O_2/balance gas N_2) through the ozone generator, and the concentration was maintained at 210 ppm. The gaseous VOCs were produced by bubbling N_2 through the liquid VOCs placed in a water bath of 1 ± 0.2 °C. The target concentration of VOCs is controlled by adjusting the N_2 flow rate, and the concentrations of toluene, formaldehyde, methanol, and ethyl acetate were 30, 100, 100, and 20 ppm, respectively. Similarly, water vapor is obtained by passing N_2 into a bubble column filled with water, and the relative humidity of the reaction gas is stabilized at 50 ± 5%.

The 0.4 g screened catalyst (40–60 mesh) was first pretreated for 30 min at 150 °C in N_2 atmosphere to remove the adsorbed water and the impurities on the surface. Then, the reaction gas was passed over the catalyst (GHSV, about 150,000 h^{-1}, unless specified) to perform the catalytic ozonation of the VOCs.

The concentration of each component in the tail gas was measured at the outlet of the reactor, and the O_3 concentration was determined by an ozone detector (2B Technologies, Boulder, CO, USA). Additionally, VOCs and CO_x were analyzed on-line by a gas chromatograph (GC-2014, Shimadzu, Japan) equipped with a hydrogen flame ionization detector (FID) and a DB-WAX capillary column (30 m × 320 μm × 0.25 μm). VOCs conversion rate, ozone decomposition rate, CO_x selectivity, and mineralization rate were calculated by Equations (1)–(4), respectively:

$$\text{VOC}_s \text{ conversion } (\%) = \frac{\text{VOC}_{s(in)} - \text{VOC}_{s(out)}}{\text{VOC}_{s(in)}} \times 100\% \quad (1)$$

$$O_3 \text{ decomposition } (\%) = \frac{O_{3(in)} - O_{3(out)}}{O_{3(in)}} \times 100\% \quad (2)$$

$$CO_x \text{ selectivity } (\%) = \frac{CO_{(out)} + CO_{2(out)}}{(\text{VOC}_{s(in)} - \text{VOC}_{s(out)}) \times n} \times 100\% \quad (3)$$

$$\text{VOC}_s \text{ mineralization rate } (\%) = \frac{CO_{2(out)}}{\text{VOC}_{s(in)} \times n} \times 100\% \quad (4)$$

where $X_{(in)}$ and $X_{(out)}$ are inlet and outlet VOCs, O_3, CO, or CO_2 concentrations, and n is the number of carbon atoms in VOCs, respectively.

3. Results and Discussion

3.1. Structure and Morphology

The XRD patterns of NiO catalysts before and after CTAB modification were depicted in Figure 1. As shown in Figure 1a, the four NiO catalysts all had the characteristic diffraction peaks of monoclinic nickel oxide (JCPDS 04-007-9781), which are located at 37.3, 43.3, 62.9, 75.4, and 79.4°, corresponding to (110), (200), (111), (021), and (220) crystal

planes. Additionally, there were no diffraction peaks of other crystal phases, indicating that the NiO catalysts before and after modification were all standard monoclinic nickel oxide. In addition, it can be found from the partial expanded figure (Figure 1b) that with the increase in CTAB concentration, the characteristic diffraction peaks of NiO catalyst gradually weaken, broaden, and shift to lower angles. This may be attributed to the impact of CTAB as a surfactant on the crystal growth process of NiO. CTAB with the positive charge can be attracted to the NiO surface with the negative charge to form a bilayer. At the same time, the hydroxyl groups of the CTAB can form hydrogen bonds with the oxygen atoms on the surface of the NiO, further enhancing the binding between them [25]. When the doping concentration of the CTAB gradually increases, the CTAB molecules continuously adsorb on the crystal face of the NiO to form an organic phase, which inhibits the growth of the NiO crystal, and resulted in the decrease of the grain size and crystallinity of the NiO and a slight lattice distortion [26,27].

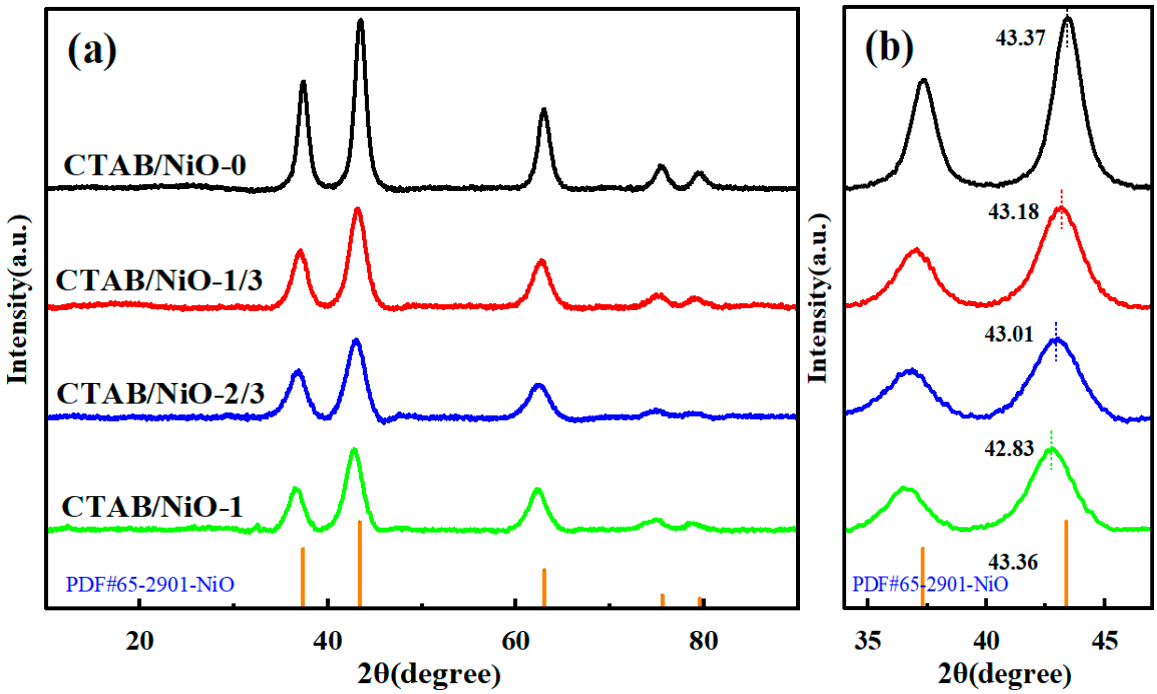

Figure 1. (**a**) XRD patterns of NiO catalysts modified with different amounts of CTAB, (**b**) partially expanded XRD patterns.

Figure 2 showed the scanning electron microscopy (SEM) images of the NiO catalysts after and before CTAB modification. As seen from Figure 2a, the NiO before modification displayed regular spheres with diameters of about 3 μm. The spheres consisted of numerous connected nanorods with a thickness of approximately 10–20 nm and a length of roughly 100–200 nm, and there existed few pores between the nanorods (Figure 2b). In contrast, the CTAB/NiO after CTAB modification exhibited a non-uniform spheroid-like structure being about 1 μm, with spheres stacking on each other (Figure 2c,e,g). Figure 2d,f,h described that the CTAB/NiO spheres were composed of nanorods with pointed ends, and the thickness of these nanorods was about 5–10 nm and the length was about 50–100 nm. Compared with the unmodified NiO, these nanorods gradually decrease in size, becoming more slender and dispersed as the CTAB doping amount increases. However, when CTAB was doped excessively (Figure 2g,h), the nanorods began to aggregate and the dispersion degree decreased.

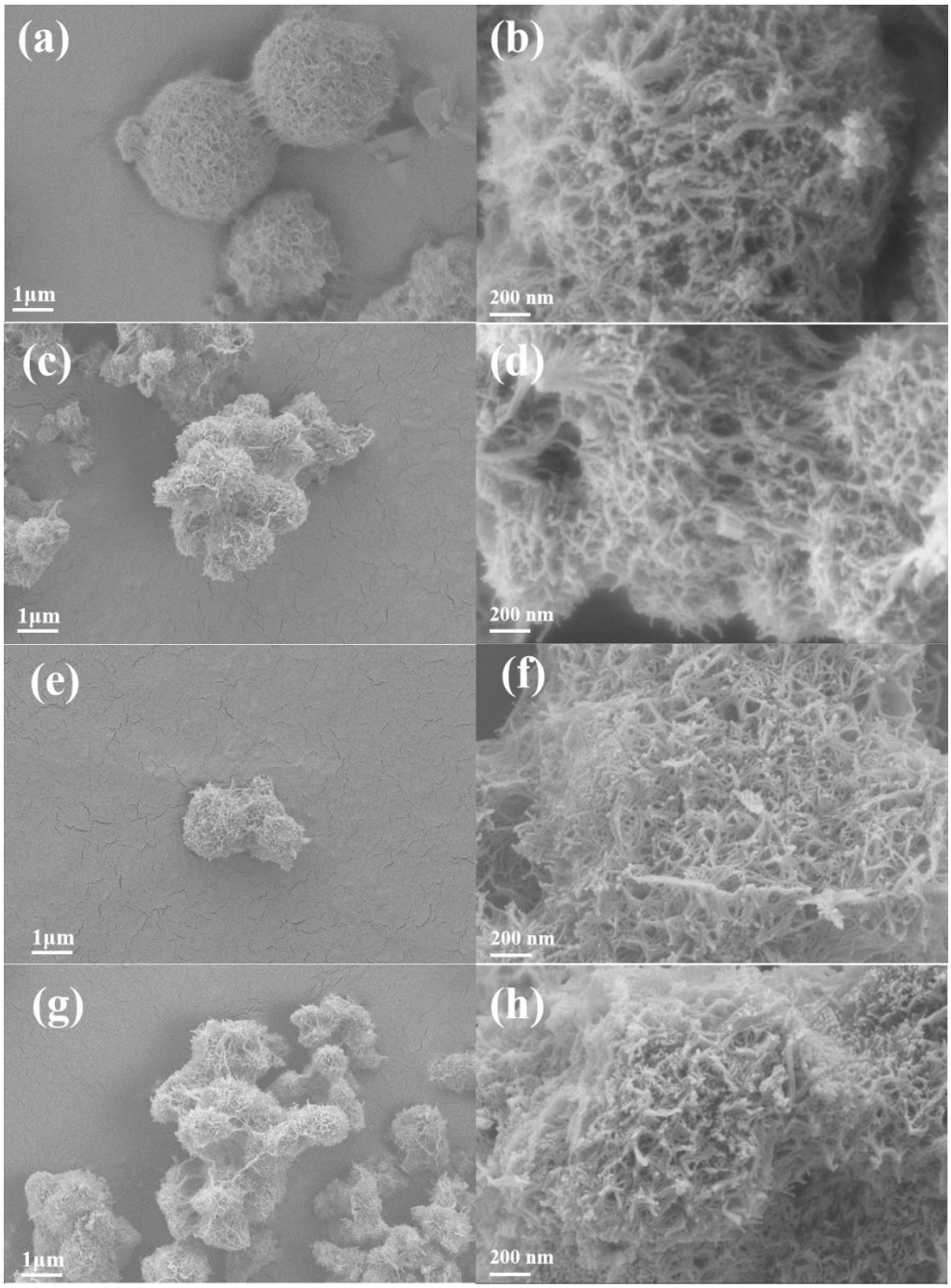

Figure 2. SEM image of NiO catalysts modified with different amounts of CTAB, (**a**,**b**) CTAB/NiO-0, (**c**,**d**) CTAB/NiO-1/3, (**e**,**f**) CTAB/NiO-2/3, and (**g**,**h**) CTAB/NiO-1.

3.2. Surface Area and Pore Structure

The N_2 adsorption isotherm and pore size distribution of the NiO catalyst are shown in Figure 3. It was found that the isotherms of the four catalysts were consistent with the type IV adsorption isotherm of the H_2 hysteresis loop in the IUPAC classification standard, suggesting that the synthesized NiO possessed abundant mesoporous structures. BET surface area and pore parameters calculated by the BJH method were listed in Table 1. The specific surface areas of CTAB/NiO-0, CTAB/NiO-1/3, CTAB/NiO-2/3, and CTAB/NiO-1 are 141.16, 163.18, 202.33, and 172.18 m^2/g, respectively. The CTAB modification enhanced the specific surface area and pore volume of the NiO catalysts. It is worth noting that the specific surface area and pore volume of CTAB/NiO-2/3 increased by 43% and 73%,

respectively (Table 1). Clearly, these findings evidenced that the CTAB doping can boost the dispersion and porosity of the CTAB/NiO-0 catalysts, resulting in an increase in their specific surface area and pore volume. It brought in more favorable active sites for the adsorption of VOCs on the catalyst surface and improved their catalytic activity for the catalytic ozonation of VOCs. However, the excessive addition of CTAB may lead to the aggregation of NiO nanorods to form a dense and inefficient structure, which reduced the specific surface area and porosity of the NiO catalyst, thereby inhibiting its catalytic performance. The results are consistent with the SEM.

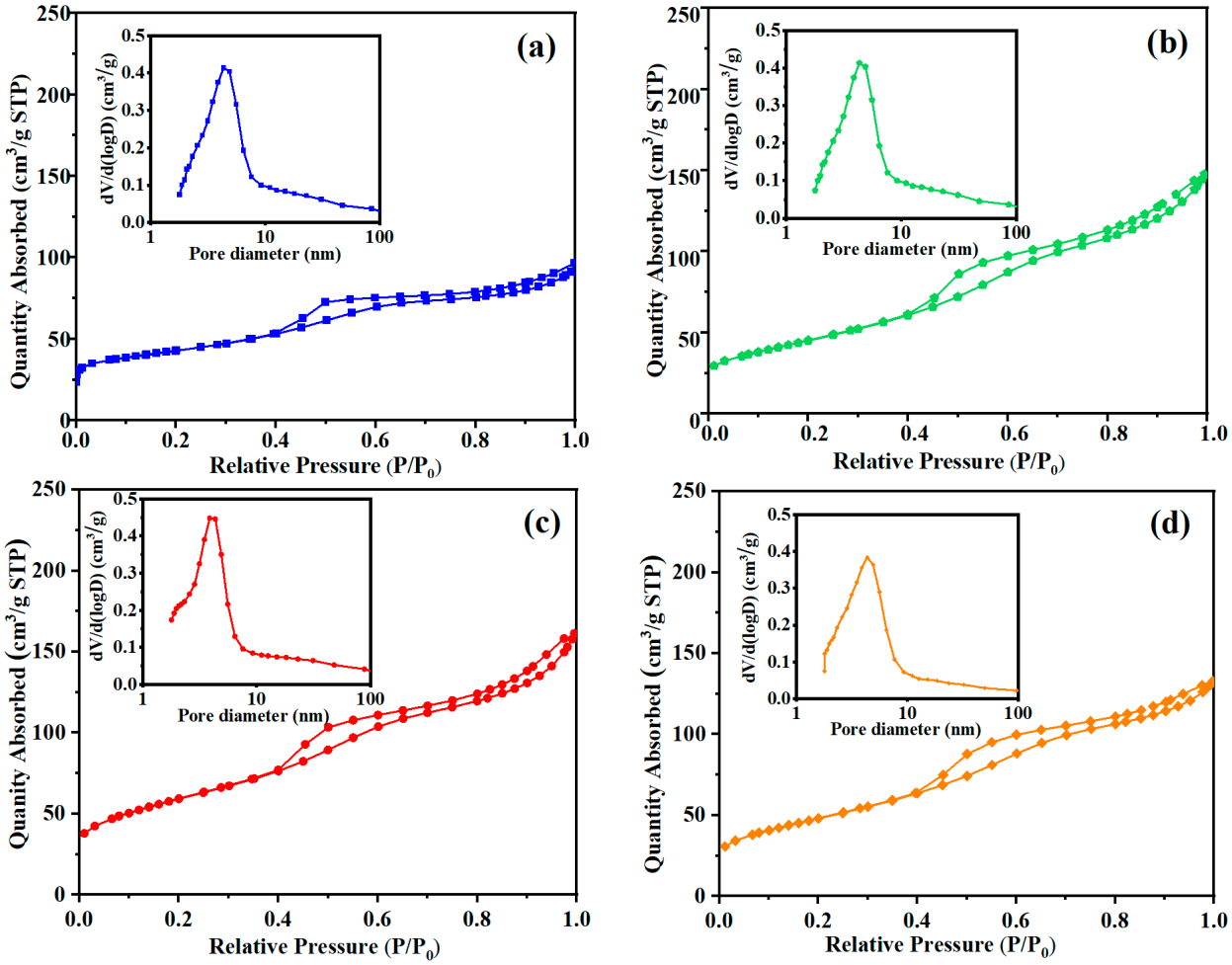

Figure 3. N_2 adsorption/desorption isotherms and pore-size distributions (inset) of (**a**) CTAB/NiO-0, (**b**) CTAB/NiO-1/3, (**c**) CTAB/NiO-2/3, and (**d**) CTAB/NiO-1.

Table 1. Specific surface area, average pore size, and pore volume of different catalysts.

Catalyst	S_{BET} (m^2/g)	Pore Size (nm)	Pore Volume (cm^3/g)
CTAB/NiO-0	141.16	5.14	0.1542
CTAB/NiO-1/3	163.18	4.85	0.2317
CTAB/NiO-2/3	202.33	4.22	0.2606
CTAB/NiO-1	172.18	4.21	0.2494

3.3. Redox Properties

H_2-TPR can be employed to investigate redox properties of different NiO catalysts. As shown in Figure 4, there was a prominent overlapping peak in the range of 100–400 °C of NiO. According to the main reduction reaction of NiO in the H_2-TPR process, this overlapping peak can be divided into two reduction peaks, corresponding to the two chemical reactions

of $Ni^{3+} \rightarrow Ni^{2+}$ and $Ni^{2+} \rightarrow Ni$, respectively. Furthermore, it can be clearly seen that the peak temperatures of the two sharp reduction peaks of Ni^{3+} and Ni^{2+} of each NiO were in the descending order of CTAB/NiO-0 > CTAB/NiO-1/3 > CTAB/NiO-1 > CTAB/NiO-2/3. As we all know, the temperature of reduction peaks usually reflects reducibility of catalysts. The reduction temperature of CTAB/NiO-2/3 was the lowest, indicating its outstanding redox ability. H_2-TPR results demonstrated that CTAB modification did indeed bring about a positive impact on the reduction performance of the NiO catalyst.

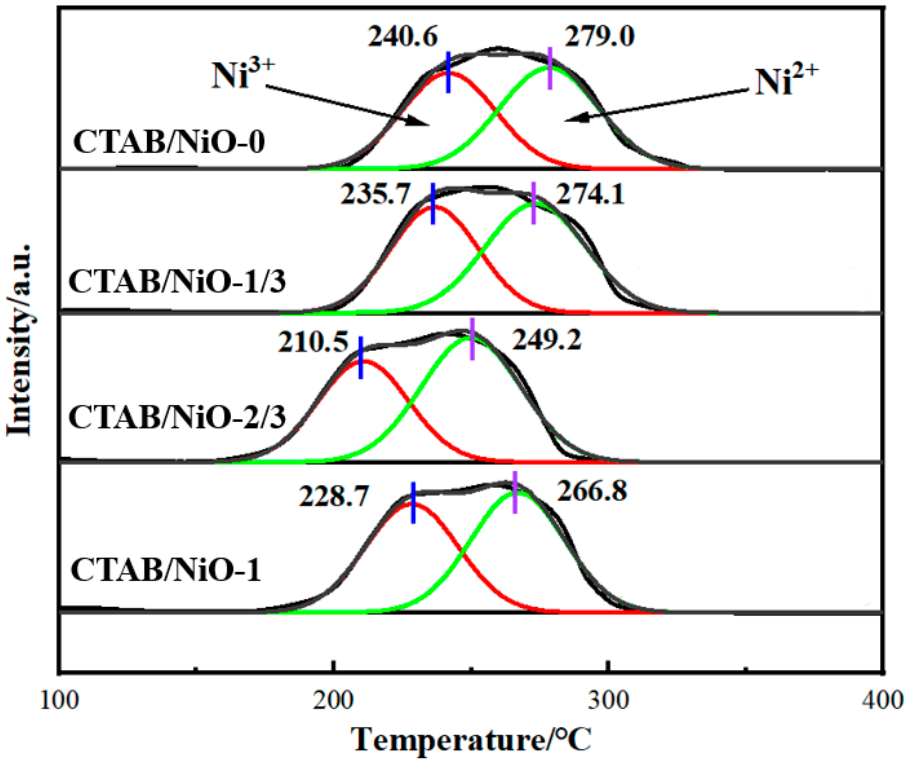

Figure 4. H_2-TPR of different catalysts.

3.4. Catalytic Performance

In this section, the catalytic activity of different concentrations of CTAB-modified NiO catalysts in the catalytic ozonation of toluene was investigated. Before testing the catalytic activity of different catalysts, adsorption experiments were conducted, and the catalyst was saturated with toluene. As shown in Figure 5, the catalytic activity of the unmodified NiO is lower than that of the modified NiO catalysts. As the reaction time increases (4 h), the toluene conversion rate and the ozone decomposition rate drop rapidly from the initial 83% and 100% to 60% and 67%, respectively. The CO_x selectivity and mineralization rate of CTAB/NiO-0 were basically maintained between 50–58% and 35–45%. The activity and stability of the CTAB/NiO-2/3 catalyst were the most excellent, and its initial toluene conversion rate reached 96%. After the reaction for 4 h, the conversion rate dropped by only 14%, while the ozone decomposition rate still remained above 95%. At the same time, during the reaction process, the CO_x selectivity and mineralization rate of CTAB/NiO-2/3 remained in the range of 70–80% and 60–70%, respectively. Compared with CTAB/NiO-0, the toluene conversion rate, ozone decomposition rate, CO_x selectivity, and mineralization rate of CTAB/NiO-2/3 were all increased by more than 20%, while that of CTAB/NiO-1/3 and CTAB/NiO-1 only improved about 10%. Combined with the BET results, it can be deduced that adding an appropriate amount of CTAB can significantly increase the specific surface area and pore volume of NiO, by which the catalytic activity could be promoted.

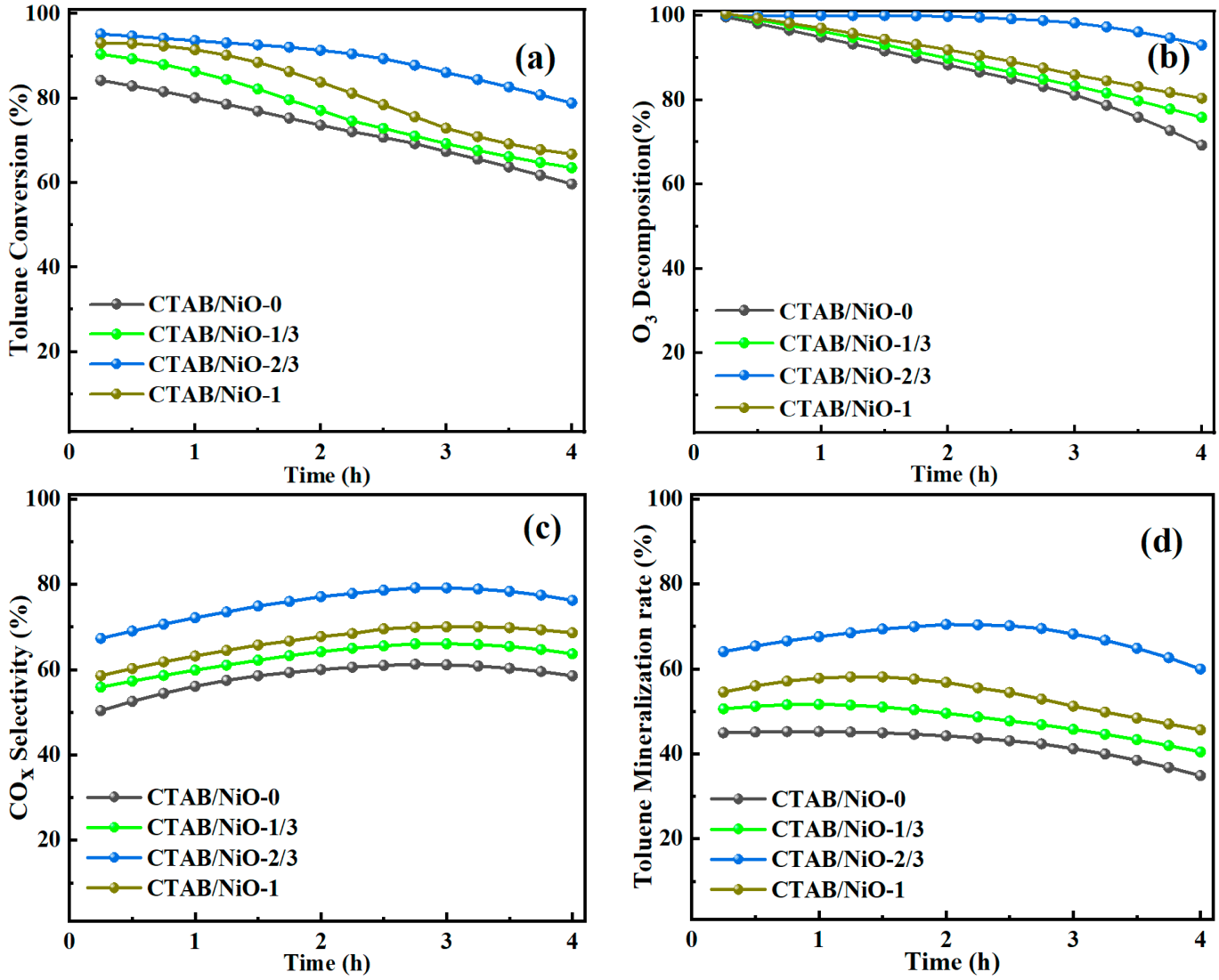

Figure 5. Catalytic activity of different catalysts. (**a**) Toluene conversion. (**b**) Ozone decomposition. (**c**) CO_x selectivity. (**d**) Toluene mineralization rate (O_3 = 210 ± 10 ppm, T = 30 ± 1 °C, C_7H_8 = 30 ± 1 ppm, RH = 50 ± 5%, GHSV = 150,000 h^{-1}).

3.5. Reaction Path

The reaction intermediate products of NiO catalysts before and after CTAB modification were determined by in situ DRIFTS (Figure 6 and Table 2), and the corresponding reaction path was deduced. The peaks at 819 and 976 cm^{-1} in the low frequency area of the in-situ DRIFTS spectra correspond to the stretching and torsional vibration peaks of C-H, respectively [28]. The peak observed around 1050 cm^{-1} was attributed to the C-O stretching vibration peak of alcohols, indicating the formation of benzyl alcohol during the catalytic ozonation of toluene [29]. The signal value of the benzaldehyde species can be observed at 1176 cm^{-1} [30], together with weak absorption peaks of maleic anhydride (1315 cm^{-1}) [28] and carboxylate (1382 cm^{-1}) [31]. The band detected at 1454 cm^{-1} is assigned to the -CH=CH- bending vibration of the benzene ring [32,33]. Generally, the bands at around 3400–3800 cm^{-1} belong to the vibration of Ni-OH and water molecules coordinated to the surface metal cations [32].

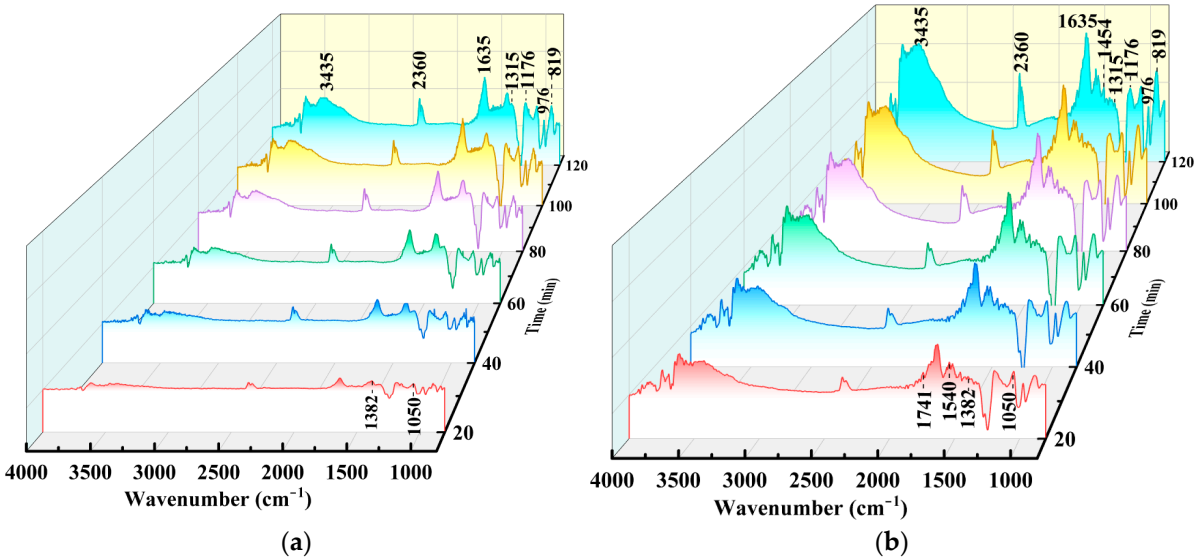

Figure 6. In situ DRIFTS spectra of catalytic ozonation of toluene over (**a**) CTAB/NiO-0, (**b**) CTAB/NiO-2/3.

Table 2. The attribution of IR bands in the catalytic ozonation of toluene.

Position (cm^{-1})	Assignment	Characteristic of
3600~3000	O-H stretching vibration	metal-OH
1741	C=O symmetrical stretching vibration	quinone
1450~1650	C=C stretching vibrations	aromatic ring
1540	C=O stretching vibrations	benzoate
1382	COO- symmetrical stretching oscillation	carboxylic acid
1315	C-C-C (O) in-plane bending vibration	maleic anhydride
1176	C-O symmetric stretching vibration	benzaldehyde
1050	C-O symmetric stretching vibration	alcohols
976	C-H torsional vibration	olefin
891	C-H stretching vibration	alkyne

In Figure 6a,b, the obvious band at 1635 cm^{-1} is denoted as stretching vibration peaks of the aromatic ring skeleton [28,34]; however, the peak intensity of CTAB/NiO-2/3 was higher than that of NiO, indicating that there were more aromatic compounds generated on the surface of CTAB/NiO-2/3. Interestingly, it can be seen in the spectrum of CTAB/NiO-2/3 that new absorption peaks around 1540 cm^{-1} and 1741 cm^{-1} were observed (Figure 6b). The more obvious absorption peak located at 1540 cm^{-1} is characteristic of the C=O antisymmetric vibration peak in benzoate species [35], which is the key intermediate involved in the oxidation of toluene. Besides, in Figure 6b, the C=O weak stretching vibration peak (1741 cm^{-1}) of quinone appeared; quinone is a kind of higher oxidation product produced by further oxidation of phenol [31,36]. Additionally, the bands at about 2360 cm^{-1} have been reported to be attributed to the stretching vibrations of C-O bonds from CO_2 [32,37]. It can be clearly seen that the CO_2 signal of CTAB/NiO-2/3 after modification was stronger than that of NiO, explaining that CTAB/NiO-2/3 can oxidize more intermediate by-products to CO_2. In short, according to in-situ DRIFTS spectra, we found that the intermediate products of CTAB/NiO-2/3 were highly oxidized under the same conditions; it is clear that the introduction of CTAB is beneficial to the catalytic oxidation performance of NiO and the deep oxidation of toluene. Therefore, we can preliminarily propose that the oxidation of toluene may follow the path: toluene→benzyl alcohol→benzaldehyde→benzoic acid→benzene→phenol→quinone, followed by ring opening to generate maleic anhydride and other small molecular species, and finally mineralization to CO_2 and H_2O.

3.6. Catalytic Ozonation of Other Typical VOCs

At present, different industrial waste gases discharge various VOCs. Besides monoaromatic hydrocarbons, being the most worrying and most emitted, there are alcohols, aldehydes, and esters, and so on [38]. More importantly, different sorts of VOCs exhibit significant differences in terms of molecular dynamic diameter, hydrophilicity, and molecular polarity, which brings considerable challenges to VOCs removal. In this section, we further investigated the degradation effects of CTAB/NiO catalysts on formaldehyde, methanol, and ethyl acetate, respectively (Figure 7a). Before testing the catalytic activity of different catalysts, the adsorption experiments were conducted, and the catalyst was saturated with VOCs. Figure 7b illustrated that NiO can completely remove ozone under the investigated reaction conditions whether the NiO was modified or not. However, the catalysts exhibited different catalytic activities for the catalytic oxidation of typical VOCs.

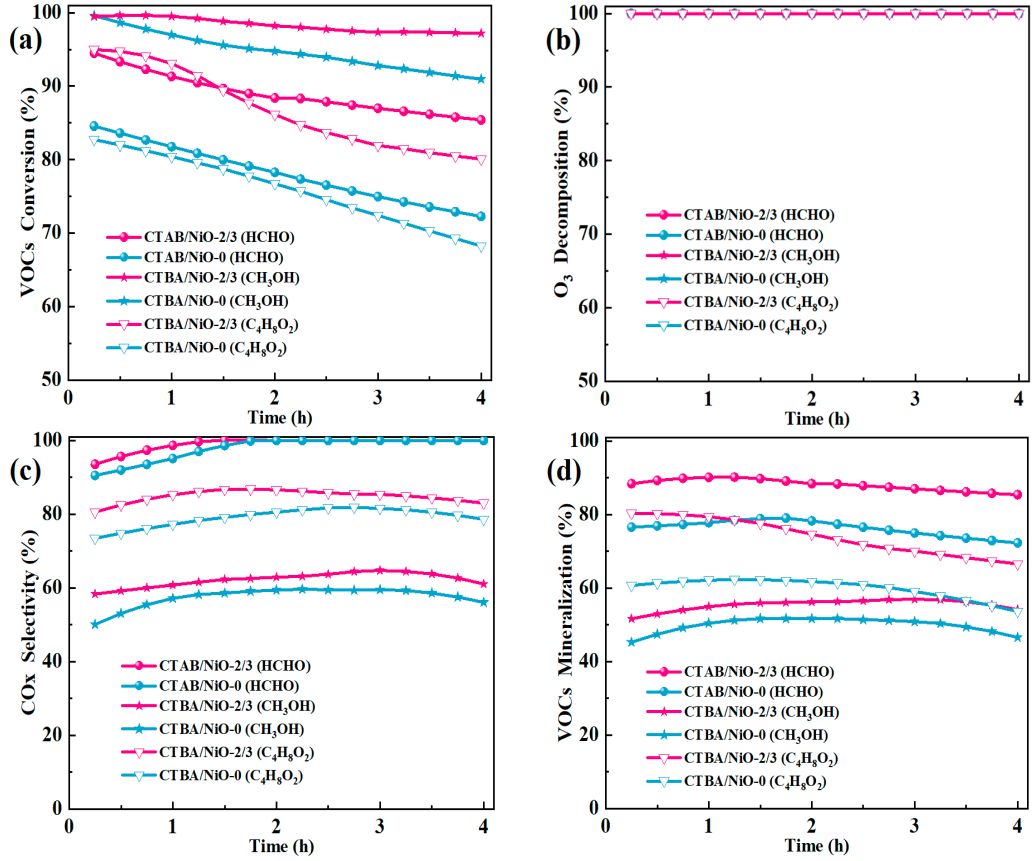

Figure 7. Catalytic activity of typical VOCs of different catalysts. (**a**) VOCs conversion. (**b**) Ozone decomposition. (**c**) CO_X selectivity. (**d**) VOCs mineralization (O_3 = 210 ± 10 ppm, T = 30 ± 1 °C, HCHO = 100 ± 5 ppm, CH_3OH = 100 ± 5 ppm, $C_4H_8O_2$ = 20 ± 2 ppm, RH = 50 ± 5%, GHSV = 150,000 h^{-1}).

HCHO (formaldehyde), the most common aldehyde VOCs, widely exists in industrial production, home decoration, automobile exhaust, etc., causing serious harm to human health and environmental quality. In the catalytic ozonation of HCHO, the initial HCHO conversion rate of CTAB/NiO-2/3 can reach 95%, which is superior to that of CTAB/NiO-0 (86%). After a 4 h reaction, the HCHO conversion rate of CTAB/NiO-2/3 decreased by less than 10% while that of CTAB/NiO-0 decreased by 14%, demonstrating that CTAB modification enhanced the catalytic stability of the catalyst. Figure 7c displayed the effects of the modification on CO_X selectivity and it can be seen that a similar trend of CO_X selectivity change occurs after modification. The HCHO mineralization rate of CTAB/NiO-2/3 was maintained at above 85% during the reaction process (Figure 7d). Catalytic ozonation of formaldehyde involves two reaction steps. First, formaldehyde is oxidized to

formic acid, i.e., $HCHO + O_3 \rightarrow HCOOH + O_2$, and then formic acid is oxidized to carbon dioxide and water, i.e., $HCOOH + O_3 \rightarrow CO_2 + O_2 + H_2O$ [39]. Due to the whole reaction having no other by-products, and formic acid can be easily completely oxidized by ozone at room temperature. Therefore, HCHO would be highly selectively oxidized into CO_2 and H_2O, maintaining a high mineralization rate [39]. At the same time, the high mineralization rate also directed that CTAB/NiO-2/3 can make full use of ozone to remove HCHO and avoid secondary pollution to the environment.

CH_3OH (methanol) is widely used in making fragrances, dyes, medicines, antifreeze, and other products. In terms of the catalytic ozonation of CH_3OH, compared with CTAB/NiO-0, the CTAB/NiO-2/3 still held on a high conversion rate of 97% after 4 h of reaction, demonstrating stronger stability (Figure 7a). However, according to the results in Figure 7c,d, CTAB/NiO-2/3 showed poor CO_x selectivity and CH_3OH mineralization efficiency, both achieving only 50–60%. During the catalytic ozonation reaction, methanol was first oxidized to formaldehyde, then formaldehyde was oxidized to formic acid, and finally further oxidized to CO_2 and H_2O. Based on the results of the previous section (Figure 7), HCHO could not be fully oxidized when the concentration ratio of $HCHO/O_3$ was about 1:2. Therefore, it can be speculated that in the catalytic ozonation reaction of methanol, the by-products (formaldehyde, formic acid) cannot be timely converted into CO_2 and H_2O, and may accumulate on the surface of the catalyst [40]. Which may account for the low CO_x selectivity and methanol conversion of CTAB/NiO-0 and CTAB/NiO-2/3.

$C_4H_8O_2$ (ethyl acetate) is a versatile fine chemical product and industrial solvent, mainly used in the manufacture of paint, artificial leather, plastic products, etc. [41,42]. As shown in Figure 7a, the initial $C_4H_8O_2$ conversion rate of CTAB/NiO-2/3 can reach 95%, which exceeded that of CTAB/NiO-0 (82%), and after a 4 h reaction, the conversion rate of CTAB/NiO-2/3 decreased to about 80%, while that of CTAB/NiO-0 decreased to 68%. Moreover, both CTAB/NiO-0 and CTAB/NiO-2/3 exhibited high CO_x selectivity over $C_4H_8O_2$ during the reaction, reaching about 75% and 80%, respectively (Figure 7c). What is more, CTAB/NiO-2/3 possessed better $C_4H_8O_2$ mineralization efficiency. Therefore, compared with CTAB/NiO-0, the modified CTAB/NiO-2/3 displayed a significant improvement in catalytic performance for typical VOCs in terms of the conversion rate, CO_x selectivity, and mineralization rate.

The oxygen-containing functionalities were also reported to enhance electron donor-accept interaction and electrostatic interaction between adsorbents and polar molecules [43]. Therefore, OVOCs (aldehydes, alcohols, and esters, etc.) tended to interact more with H_2O, which reduced the adsorption capacity of OVOCs and H_2O on the catalyst surface, and also weakened the competitive adsorption of O_3 and H_2O. This was the reason why the ozone degradation rate in the catalytic ozonation of aldehydes, alcohols, and esters was superior to that in the catalytic ozonation of toluene.

4. Conclusions

In our work, a series of CTAB-modified NiO catalysts were prepared using a thermal solvent method and modified with CTAB as a crystal structure-directing agent. The effect of CTAB on the catalytic ozonation performance of the NiO catalysts was investigated. XRD analysis revealed that both pristine and CTAB-modified NiO have a monoclinic structure. BET and H_2-TPR results showed that the introduction of CTAB was beneficial to the enhancement of surface area and redox properties. CTAB/NiO-2/3 exhibited the best catalytic activity in catalytic ozonation of toluene at room temperature (30 °C), which was superior to unmodified NiO. What is more, according to in situ DRIFTS, it is clear that the by-products on the CTAB/NiO-2/3 surface were oxidized to a higher degree, which contributed to the oxidation of toluene to CO_2 and H_2O. Additionally, CTAB modification could significantly enhance the catalytic ozonation performance for formaldehyde, methanol, and ethyl acetate.

Author Contributions: Conceptualization, C.A. and X.J.; Methodology, X.J. and W.H.; Validation, Y.S. and T.Z.; Formal analysis, W.H. and Y.S.; Investigation, C.A., X.J. and Y.S.; Resources, T.Z.;

Writing—original draft, C.A.; Writing—review & editing, T.Z. All authors have read and agreed to the published version of the manuscript.

Funding: This research was funded by National Natural Science Foundation of China (No. 52070010).

Data Availability Statement: The data discussed in this work are presented in the form of tables and figures in the article, and no data are withheld. All of the data can be accessed from the journal article.

Conflicts of Interest: The authors declare no conflict of interest.

References

1. Huang, R.J.; Zhang, Y.L.; Bozzetti, C.; Ho, K.F.; Cao, J.J.; Han, Y.; Daellenbach, K.R.; Slowik, J.G.; Platt, S.M.; Canonaco, F.; et al. High Secondary Aerosol Contribution toParticulate Pollution During Haze Events in China. *Nature* **2014**, *514*, 218–222. [CrossRef]
2. Suzuki, N.; Nakaoka, H.; Nakayama, Y.; Tsumura, K.; Takaguchi, K.; Takaya, K.; Eguchi, A.; Hanazato, M.; Todaka, E.; Mori, C. Association Between Sum of Volatile Organic Compounds and Occurrence of Building-Related Symptoms in Humans: A Study in Real Full-scale Laboratory Houses. *Sci. Total Environ.* **2021**, *750*, 141635. [CrossRef]
3. Peel, A.M.; Wilkinson, M.; Sinha, A.; Loke, Y.K.; Fowler, S.J.; Wilson, A.M. Volatile Organic Compounds Associated with Diagnosis and Disease Characteristics in Asthma-A Systematic Review. *Res. Med.* **2020**, *169*, 105984. [CrossRef]
4. Mesquita, A.S.; Zamora-Obando, H.R.; Santos, F.N.; Schmidt-Filho, J. Volatile organic compounds analysis optimization and biomarker discovery in urine of Non-Hodgkin lymphoma patients before and during chemotherapy. *Microchem. J.* **2020**, *159*, 105479. [CrossRef]
5. Li, T.; Li, H.; Li, C.L. A Review and Perspective of Recent Research in Biological Treatment Applied in Removal of Chlorinated Volatile Organic Compounds from Waste Air. *Chemosphere* **2020**, *250*, 126338. [CrossRef] [PubMed]
6. Blanch, A.; Bianchi, A.C.; Leach, J. Volatile organic compounds in an urban airborne environment adjacent to a municipal incinerator, waste collection centre and sewage treatment plant. *Atmos. Environ.* **1999**, *23*, 4309–4325.
7. Dimosthenis, A.; Sarigiannis, S.P.; Karakitsios, A.G. Exposure to Major Volatile Organic Compounds and Carbonyls in European Indoor Environments and Associated Health Risk. *Environ. Int.* **2011**, *37*, 743–765.
8. Lu, Y.Q.; Deng, H.; Pan, T.T.; Zhang, C.B.; He, H. Thermal Annealing Induced Surface Oxygen Vacancy Clusters in α-MnO_2 Nanowires for Catalytic Ozonation of VOCs at Ambient Temperature. *ACS Appl. Mater. Interfaces* **2023**, *15*, 9362–9372. [CrossRef] [PubMed]
9. Peng, S.P.; Ma, Z.R.; Ma, J.; Wang, H.Y.; Ren, K.; Wu, X.D.; Wang, B.D. In Situ DRIFTS Study of Single-Atom, 2D, and 3D Pt on γ-Al_2O_3 Nanoflakes and Nanowires for C_2H_4 Oxidation. *Processes* **2022**, *10*, 1773. [CrossRef]
10. Zhang, Z.X.; Jiang, Z.; Shangguan, W.F. Low-temperature Catalysis for VOCs Removal in Technology and Application: A state-of-the-art Review. *Catal. Today* **2016**, *264*, 270–278. [CrossRef]
11. Xu, Z.Y.; Mo, S.P.; Li, Y.X.; Zhang, Y.C.; Wu, J.L.; Fu, M.L.; Niu, X.J.; Hu, Y.; Ye, D.Q. Pt/MnO_x for Toluene Mineralization via Ozonation Catalysis at Low Temperature: SMSI Optimization of Surface Oxygen Species. *Chemosphere* **2022**, *286*, 131754. [CrossRef]
12. An, C.G.; Jiang, X.X.; Hong, W.; Zhu, T.L.; Sun, Y.; Li, X.; Shen, F.X. Synergistic Promotion Effects of Surface Hydroxyl Groups (-OH) and Nitrate Groups (-NO_3) on Catalytic Ozonation of Toluene over MnFe Catalyst. *Appl. Catal. A-Gen.* **2023**, *654*, 119078. [CrossRef]
13. Tian, S.H.; Zhan, S.J.; Lou, Z.C.; Zhu, J.Z.; Feng, J.X.; Xiong, Y. Electrodeposition Synthesis of 3D-$NiO_{1-\delta}$ Flowers Grown on Ni Foam Monolithic Catalysts for Efficient Catalytic Ozonation of VOCs. *J. Catal.* **2021**, *398*, 1–13. [CrossRef]
14. Wang, Z.; Xie, K.Y.; Zheng, J.; Zuo, S.F. Studies of Sulfur Poisoning Process via Ammonium Sulfate on MnO_2/γ-Al_2O_3 Catalyst for Catalytic Combustion of Toluene. *Appl. Catal. B-Environ.* **2021**, *298*, 120595. [CrossRef]
15. Zhang, W.X.; Xue, M.; Fan, J.; Qiu, L.L.; Zheng, W.X.; Liu, Y.Y.; Meng, Z.H. Flory-Huggins VOC Photonics Sensor Made of Cellulose Derivatives. *ACS Appl. Mater. Interfaces* **2022**, *14*, 10701–10711. [CrossRef]
16. Lou, B.Z.; Shakoor, N.; Adeel, M.; Zhang, P.; Huang, L.L.; Zhao, Y.W.; Zhao, W.C.; Jiang, Y.Q.; Rui, Y.K. Catalytic Oxidation of Volatile Organic Compounds by Non-noble Metal Catalyst: Current Advancement and Future Prospectives. *J. Clean. Prod.* **2022**, *363*, 132523. [CrossRef]
17. Ádám, A.A.; Ziegenheim, S.; Papp, Á.; Szabados, M.; Kónya, Z.; Kukovecz, Á.; Varga, G. Nickel Nanoparticles for Liquid Phase Toluene Oxidation-Phenomenon, Opportunities and Challenges. *ChemCatChem* **2022**, *14*, e20220070. [CrossRef]
18. Peng, J.L.; Lai, L.D.; Jiang, X.; Jiang, W.J.; Lai, B. Catalytic Ozonation of Succinic acid in Aqueous Solution using the Catalyst of Ni/Al_2O_3 Prepared by Electroless Plating-calcination Method. *Sep. Purif. Technol.* **2018**, *195*, 138–148. [CrossRef]
19. Zhan, S.J.; Hu, X.N.; Lou, Z.C.; Zhu, J.Z.; Xiong, Y.; Tian, S.H. In-situ Growth of Defect-enriched NiO Film on nickel Foam (NF@NiO) Monolithic Catalysts for Ozonation of Gaseous Toluene. *J. Alloy. Compd.* **2022**, *893*, 162160. [CrossRef]
20. Rodríguez, J.L.; Valenzuela, M.A.; Poznyak, T.; Lartundo, L.; Chairez, I. Reactivity of NiO for 2,4-D Degradation with Ozone: XPS Studies. *J. Hazard. Mater.* **2013**, *262*, 472–481. [CrossRef]
21. Stoyanova, M.; Konova, P.; Nikolov, P.; Naydenov, A.; Christoskova, S.; Mehandjiev, D. Alumina-supported Nickel Oxide for Ozone Decomposition and Catalytic Ozonation of CO and VOCs. *Chem. Eng. J.* **2006**, *122*, 41–46. [CrossRef]

22. Kaur, N.; Singh, J.; Kaur, G. CTAB Assisted Co-precipitation Synthesis of NiO Nanoparticles and their Efficient Potential towards the Removal of Industrial Dyes. *Micro Nano Lett.* **2019**, *14*, 856–859. [CrossRef]
23. Lu, W.T.; Zhang, G.; Wei, F.; Li, W.H.; Cheng, K.; Ding, F.; Zhang, J.Y.; Zheng, W.Q. Shape-Controlled Synthesis of Pd Nanocrystals in Aqueous Solutions. *Adv. Funct. Mater.* **2009**, *19*, 2–3.
24. Tong, J.X.; Wang, J.; Huang, H.X. Surfactant-Assisted Synthesis of $LiNi_{0.8}Co_{0.1}Mn_{0.1}O_2$ Cathode Material. *Chin. J. Inorg. Chem.* **2021**, *37*, 835–843.
25. Tawfik, S.M.; Negm, N.A.; Bekheit, M.; El-Rahman, N.R.A.; Abd-Elaal, A.A. Synergistic Interaction in Cationic Antipyrine/CTAB Mixed Systems at Different Phases. *J. Disper. Sci. Technol.* **2021**, *35*, 835–843. [CrossRef]
26. Li, X.T.; Ma, J.Z.; Yang, L.; He, G.Z.; Zhang, C.B.; Zhang, R.D.; He, H. Oxygen Vacancies Induced by Transition Metal Doping in γ-MnO_2 for Highly Efficient Ozone Decomposition. *Environ. Sci. Technol.* **2018**, *52*, 12685–12696. [CrossRef] [PubMed]
27. Yu, H.W.; Wang, J.; Xia, C.J.; Yan, X.A.; Cheng, P.F.; Liu, H.C.; Wang, C.L.; Duan, B.R. Preparation and Photocatalytic Characterization of Flower-like ZnO via CTAB Assisted Hydrothermal Synthesis. *Basic Sci. J. Text. Univ.* **2017**, *30*, 541–546.
28. Yang, X.Q.; Yu, X.L.; Jing, M.Z.; Song, W.Y.; Liu, J.; Ge, M.F. Defective $Mn_xZr_{1-x}O_2$ Solid Solution for the Catalytic Oxidation of Toluene: Insights into the Oxygen Vacancy Contribution. *ACS Appl. Mater. Interfaces* **2018**, *11*, 730–739. [CrossRef]
29. Mo, S.P.; Zhang, Q.; Li, J.Q.; Sun, Y.H.; Ren, Q.M.; Zou, S.B.; Zhang, Q.; Lu, J.H.; Fu, M.L.; Mo, D.Q.; et al. Highly Efficient Mesoporous MnO_2 Catalysts for the Total Toluene Oxidation: Oxygen-Vacancy Defect Engineering and Involved Intermediates using in situ DRIFTS. *Appl. Catal. B-Environ.* **2020**, *264*, 118464. [CrossRef]
30. Zhao, S.; Hu, F.Y.; Li, J.H. Hierarchical Core-Shell Al_2O_3@Pd-CoAlO Microspheres for Low-Temperature Toluene Combustion. *ACS Catal.* **2016**, *6*, 3433–3441. [CrossRef]
31. Liu, X.L.; Zeng, J.L.; Shi, W.B.; Wang, J.; Zhu, T.Y.; Chen, Y.F. Catalytic Oxidation of Benzene over Ruthenium-cobalt Bimetallic Catalysts and Study of its Mechanism. *Catal. Sci. Technol.* **2017**, *7*, 213–221. [CrossRef]
32. Zhong, J.P.; Zeng, Y.K.; Chen, D.D.; Mo, S.P.; Zhang, M.Y.; Fu, M.L.; Wu, J.L.; Su, Z.X.; Chen, P.R.; Ye, D.Q. Toluene Oxidation over Co^{3+}-rich Spinel Co_3O_4: Evaluation of Chemical and by-product Species Identified by in situ DRIFTS Combined with PTR-TOF-MS. *J. Hazard. Mater.* **2020**, *386*, 121957. [CrossRef] [PubMed]
33. Li, J.; Na, H.B.; Zeng, X.L.; Zhu, T.L.; Liu, Z.M. In situ DRIFTS Investigation for the Oxidation of Toluene by Ozone over Mn/HZSM-5, Ag/HZSM-5 and Mn-Ag/HZSM-5 Catalysts. *Appl. Surf. Sci.* **2014**, *311*, 690–696. [CrossRef]
34. Chen, X.; Cai, S.C.; Chen, J.; Xu, W.J.; Jia, H.P.; Chen, J. Catalytic Combustion of Toluene over Mesoporous Cr_2O_3-supported Platinum Catalysts Prepared by in situ Pyrolysis of MOFs. *Chem. Eng. J.* **2018**, *334*, 768–779. [CrossRef]
35. Sun, H.; Liu, Z.G.; Chen, S.; Quan, X. The Role of Lattice Oxygen on the Activity and Selectivity of the OMS-2 Catalyst for the Total Oxidation of Toluene. *Chem. Eng. J.* **2015**, *270*, 58–65. [CrossRef]
36. Shao, Q.; Wei, S.S.; Hu, X.Y.; Dong, H.; Wen, T.C.; Gao, L.; Long, C. Tuning the Micro-coordination Environment of Al in Dealumination Y Zeolite to Enhance Electron Transfer at the Cu-Mn Oxides Interface for Highly Efficient Catalytic Ozonation of Toluene at Low Temperatures. *Environ. Sci. Technol.* **2022**, *56*, 15449–15459. [CrossRef]
37. Tang, H.R.; He, Y.; Lin, F.W.; Zhu, Y.Q.; Duan, Y.X.; Wang, Z.H. Simultaneous Catalytic Ozonation of NO and Dichloromethane on Mn/H-ZSM-5 Catalysts: Interaction effect and mechanism. *Proc. Combust. Inst.* **2022**, *39*, 4387–4397. [CrossRef]
38. Zhang, T.; Lang, X.Y.; Dong, A.Q.; Wan, X.; Gao, S.; Wang, L.; Wang, L.X.; Wang, W.C. Difference of Oxidation Mechanism between Light C3-C4 Alkaneand Alkene over Mullite YMn_2O_5 Oxides' Catalyst. *ACS Catal.* **2020**, *10*, 7269–7282. [CrossRef]
39. Wang, L.C.; Huang, Z.W.; Jiang, Z.; Jiang, Z.; Zhang, Y.; Zhang, Z.X.; Shangguan, W.F. Trifunctional C@MnO Catalyst for Enhanced Stable Simultaneously Catalytic Removal of Formaldehyde and Ozone. *ACS Catal.* **2018**, *8*, 3164–3318. [CrossRef]
40. Tian, M.Z.; Liu, S.J.; Wang, L.L.; Ding, H.; Zhao, D.; Wang, Y.Q.; Cui, J.H.; Fu, J.F.; Shang, J.; Li, G.K. Complete Degradation of Gaseous Methanol over Pt/FeOx Catalysts by Normal Temperature Catalytic Ozonation. *Environ. Sci. Technol.* **2020**, *54*, 1938–1945. [CrossRef]
41. Li, J.; Mo, S.P.; Ding, X.G.; Huang, L.L.; Zhou, X.B.; Fan, Y.M.; Zhang, Y.N.; Fu, M.M.; Xie, Q.L.; Ye, D.Q. Hollow Cavity Engineering of MOFs-derived Hierarchical MnO_x Structure for Highly Efficient Photothermal Degradation of Ethyl Acetate under Light Irradiation. *Chem. Eng. J.* **2023**, *464*, 142412. [CrossRef]
42. Shen, Z.D.; Gao, E.G.; Meng, X.Y.; Xu, J.C.; Sun, Y.; Zhu, J.L.; Li, J.; Wu, Z.L.; Wang, W.; Yao, S.L.; et al. Mechanistic Insight into Catalytic Combustion of Ethyl Acetate on Modified CeO_2 Nanobelts: Hydrolysis-Oxidation Process and Shielding Effect of Acetates/Alcoholates. *Environ. Sci. Technol.* **2023**, *57*, 3864–3874. [CrossRef] [PubMed]
43. Yang, C.T.; Miao, G.; Pi, Y.H.; Xia, Q.B.; Wu, J.L.; Li, Z.; Xiao, J. Abatement of Various Types of VOCs by Adsorption/catalytic Oxidation: A review. *Chem. Eng. J.* **2019**, *370*, 1128–1153. [CrossRef]